Developmental Cell, Volume *41*

Supplemental Information

ER Membrane Phospholipids and Surface Tension Control Cellular Lipid Droplet Formation

Kalthoum Ben M'barek, Dalila Ajjaji, Aymeric Chorlay, Stefano Vanni, Lionel Forêt, and Abdou Rachid Thiam

Figure S1: Energy of LD vesicular budding mode and *in vitro* reconstitution, related to Figure 1 and Movie S2

(A) Surface tension measurement principle by using a micropipette approach. Pictures shown correspond to the measurement of the surface tensions of GFP-PLIN1 and mCherry-LSD1 LDs respectively purified from Cos7 and Drosophila cells. Scale bar is 10 µm.

(B) Estimation of the minimal energy to provide in function of surface tension, for the budding LDs of different sizes. This minimal energy is considered as $E = 8\pi\kappa + 4\pi r^2\gamma$ where κ (taken here as 10 k_BT) denotes for the membrane bending modulus and γ the surface tension. The band represents the range of STs of purified LDs from various cell types. For comparison, the energy provided by classical coat proteins for budding 50-100nm sized vesicles, such as complex protein I (COPI) and clathrin coats, is delineated by the horizontal line.

(C) Illustration of the giant unilamellar vesicle (GUV) and artificial LD system. The rhodamine-PE fluorescence signal on the GUV relocates to the embedded artificial LDs. Scale bar is 10 µm.

(D) Variant approach for changing the GUV phospholipid composition. GUVs made exclusively with phosphatidyl choline (PC) are mixed with artificial LDs that contain the phospholipid of interest and NBD-PE (1% w/w to phospholipids). The NDB signal relocates to the GUV membrane, suggesting that phospholipids on the droplet relocate also to the GUV. Scale bar is 10 µm.

(E) The presence of oleic acid (OA) in the GUV and artificial LD made of triolein leads to the spreading of the droplet (the droplet is on the GUV apex). The subsequent addition in the medium of active bovine serum albumin captures free oleic acid molecules. The concentration of free oleic acid molecules on the membrane decreases and leads to the budding of the artificial LD (n=5).

(F) The evolution of the artificial LD projected size during these manipulations is determined. Scale bar is 20 µm.

Figure S2: Droplet interface bilayer formation and characterization, related to Figure 2

(A) Formation kinetics of droplet interface bilayers having different equilibrium budding angles. The equilibrium angles are here reached after few seconds. Drop size is around 200 µm.

(B) Examples of droplet interface bilayers made with other surfactants and neutral lipids. Scale bar is 20 µm.

(C) Replacing triolein by trioctanoate as the neutral lipid phase has no effect on the budding angle.

(D) Quantification of the droplet interface bilayer budding angles for other surfactants in a triolein lipid phase. Lyso-PC* corresponds to a mixture of Lyso-PC with PA at 20/80. DPPC* corresponds to a mixture of DPPC with PA at 75/25.

(E) Nomenclature of the used abbreviations.

Figure S3: Triolein egress from different phospholipid bilayer environments, related to Figure 3

(A-D) Additional examples of PE and PC droplet interface bilayers, as in Figure 3A, with the triolein signal respectively present or excluded from the bilayer (B, D). Scale bars are 50 µm.

(E) GUVs made with PC/PE (50/50) are mixed with artificial LDs containing triolein and 5% Triolein-pyrene (TO-pyrene). The TO-pyrene signal relocates to the GUV membrane. (F) When GUVs are exclusively made with PC, the TO-pyrene signal is often absent from the GUV bilayer. Scale bar is 10 µm.

(G) Increase of the droplet interface bilayer budding angle due to the addition of PC-in-triolein in the surrounding bulk phase. Rhodamine-PE reports the monolayer and bilayer membranes. Scale bar is 30 µm.

(H) The decrease of the Triolein-pyrene signal in the droplet interface bilayer, due to PC addition, is concomitant to the increase of the budding angle (Figure 3D). Scale bar is 50 µm.

Figure S4: Measure of the surface tensions of different monolayer and droplet interface bilayers, related to Figure 4

(A) Principle of the monolayer surface tension measurement by the pendant drop technique. A lipid drop covered by the studied lipid surfactant is formed in a buffer phase. After equilibrium is reached (first plateau), the monolayer is compressed until a plateau of surface tension is reached (second plateau), which corresponds to the full monolayer packing; for some surfactants such as dioleylglycerol, the first and second plateaus coincide. Examples of different lipid conditions are shown. The surface tension of the second plateau is defined as the monolayer surface tension γ_m; this

is because drops are generated *in vitro* under conditions of excess surfactant to ensure maximum monolayer packing. Each measure was repeated three times.
(B) Monolayer tensions for different PC/PE ratios.
(C) The droplet interface bilayer surface tension for the different PC/PE. It is given by the corresponding monolayer tension (B), the budding angle (not shown), and the Young equation.
(D) Triolein concentration in the droplet interface bilayer increases with the monolayer tension.
(E) *In silico* determination of the concentration of free triolein molecules in the bilayer in function of the bilayer surface tension. After few nano-sec, the equilibrium concentration of free triolein in the bilayer in attained. Measurements presented in Figure 4E were conducted after 1.5µsec, which ensures equilibrium.
(F) The budding angle is presented against the monolayer surface tension of the different lipid compositions tested in Figure 2. The budding transition with the monolayer tension is less clear as with the bilayer tension (Figure 4G).

Figure S5: Dynamic remodeling of membrane phospholipid and tension for artificial lipid droplet budding, related to Figure 5
(A) Thin layer chromatography shows that the phospholipase A2 converts DOPC from liposomes into Lyso-PC; the fraction of Lyso-PC generated is beneath 15%, as revealed by the band signal (B). Addition of adenosine triphosphate (ATP) does not enhance the action of the phospholipase.
(C) PC/Lyso-PC GUVs are fabricated by using different phospholipid ratios. Above 20% Lyso-PC, no GUV is formed (1: more than 50 GUVs are observed; 0: less than 20 GUVs are observed).
(D) Phospholipase A2 induced the budding of artificial LDs from the GUV membrane, as compared to the control.
(E) Evolution of the LD projected diameter over the incubation time with or without PLA2.
(F) Measure with the microaspiration technique of the surface tension of a GUV containing an artificial LD, before and after PLA2 action. The image shown is the “top” view of the image in Figure 5E.
(G) Values of the surface tensions. These values are very likely due to the use of PA and the presence of triolein in the bilayer.
(H) Another example of the side view of the budding of an artificial LD after PLA2 action.
(I) Illustrative diagram of the topology used for developing the physical model.

Figure S6: Characterization of cellular lipid droplet size distribution upon phospholipid and neutral lipid modulation, related to Figure 6
(A) Main phenotypes of LDs, ER and neutral lipids, caused by the modulation of different proteins. There is systematically a concomitant modification of phospholipids or lipids, which could explain the alteration of LD formation.
(B-E) Histograms of the fitting curves shown in Figure 7D, 7G, 7J, and 7N; few thousands of LD size were quantified for each probed condition.
(F) The siRNA of LPCAT1 in Hela cells favors the formation of LDs slightly bigger than in WT (G, H). Scale bar is 10 µm.
(I) The double inhibition of LPCAT1, by siRNA, and ATX/Lyso-PLD, by the autotaxin inhibitor, decreases LD size distribution in a dose-dependent manner.
(J) The occurrence of big LDs in MAFP (Figure 6F) could be due to the accumulation of PA or diacylglycerols, and not to the lack of Lyso-PC. Indeed, PC is transformed to PA by the phospholipase D, which is blocked by 1-butanol. The treatment of cells with MAFP and 1-butanol still leads to bigger LDs than in WT (K, L), supporting that the MAFP phenotype is due to the lack of Lyso-PC. Scale bar is 10 µm.
(M) Thin layer chromatography shows, in mevalonic acid loading, the deposition of sterol esters. Terbinafine treatment leads to squalene deposition.

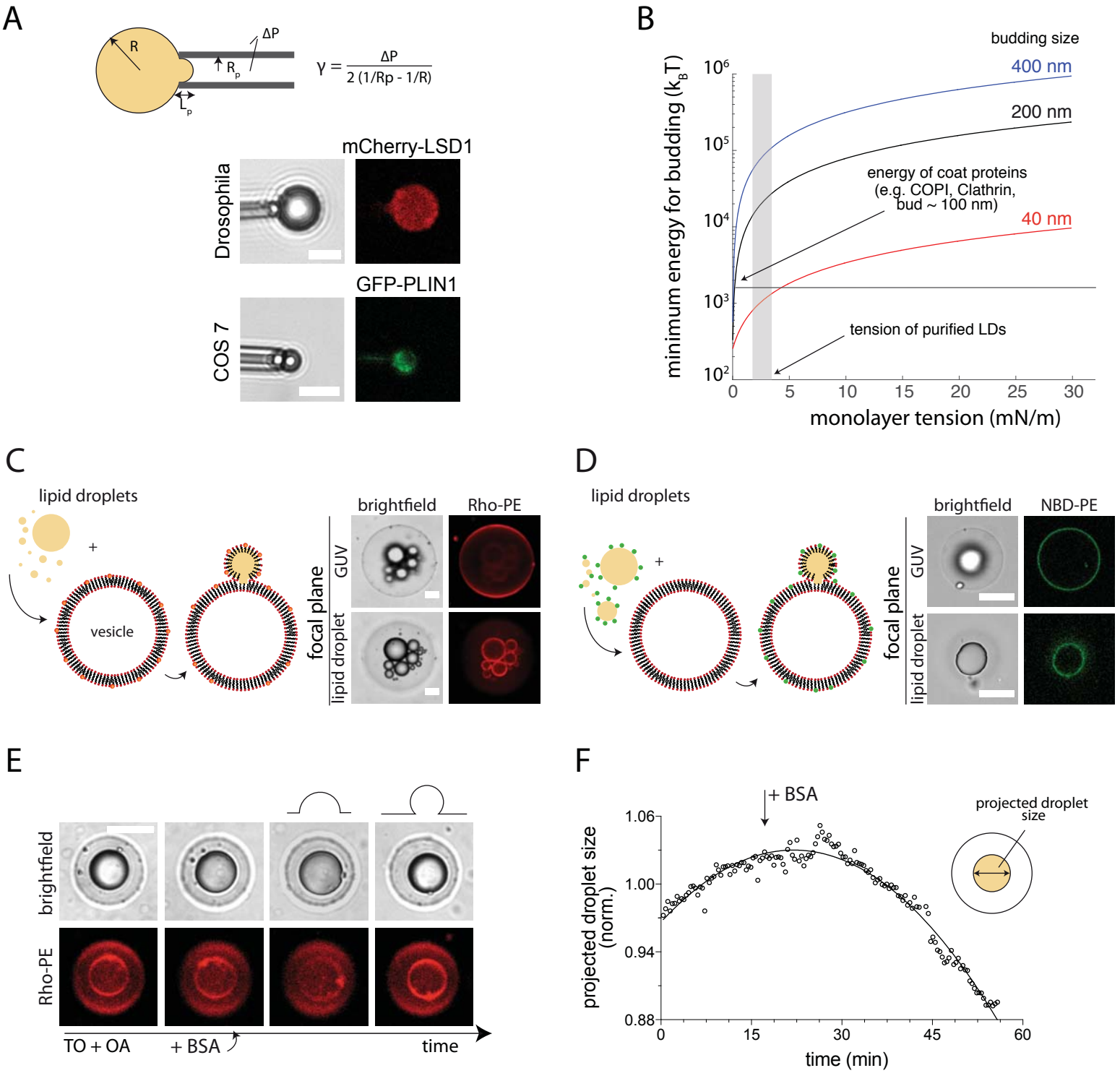

Figure S1

Ben M'Barek et al. 2016

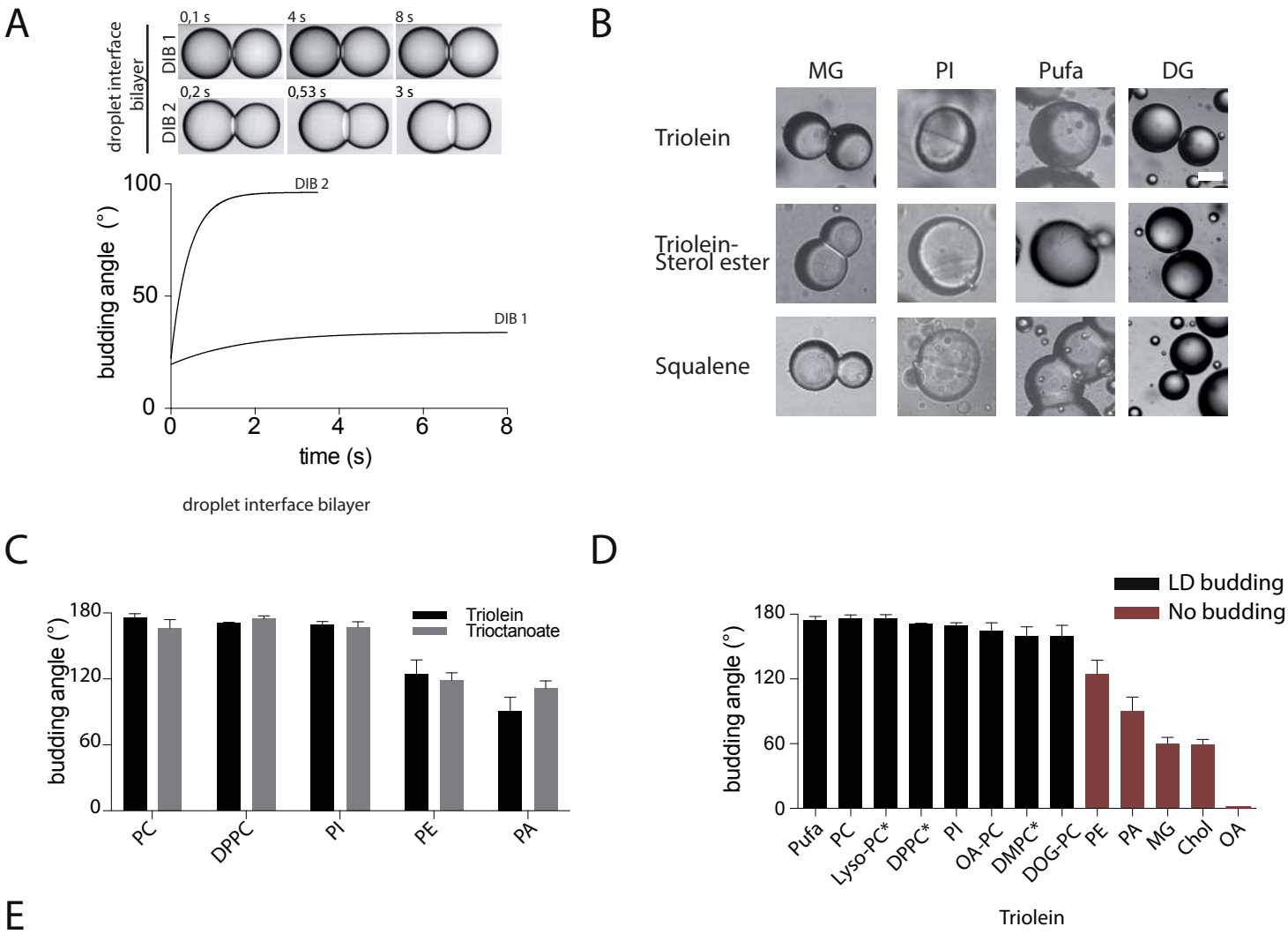

Phospholipid nomenclature

MG : mono-acylglycerol (1-(7Z-tetradecenoyl)-rac-glycerol)
DG : di-acylglycerol (1-2-dioleoyl-sn-glycerol (18:1))
Pufa : 1-stearoyl-2-docosahexaenoyl-sn-glycero-3-phosphocholine (18:0-22:6 PC)
OA : oleic acid
Chol : cholesterol
DMPC : 1,2-dimyristoyl-sn-glycero-3-phosphocholine (14:0)
DPPC : 1,2-dipalmitoyl-sn-glycero-3-phosphocholine (16:0)
Lyso-PC : 1-(1Z-octadecenyl)-sn-glycero-3-phosphocholine (C18)
PA : 1,2-dioleoyl-sn-glycero-3-phosphate (sodium salt) (18:1)

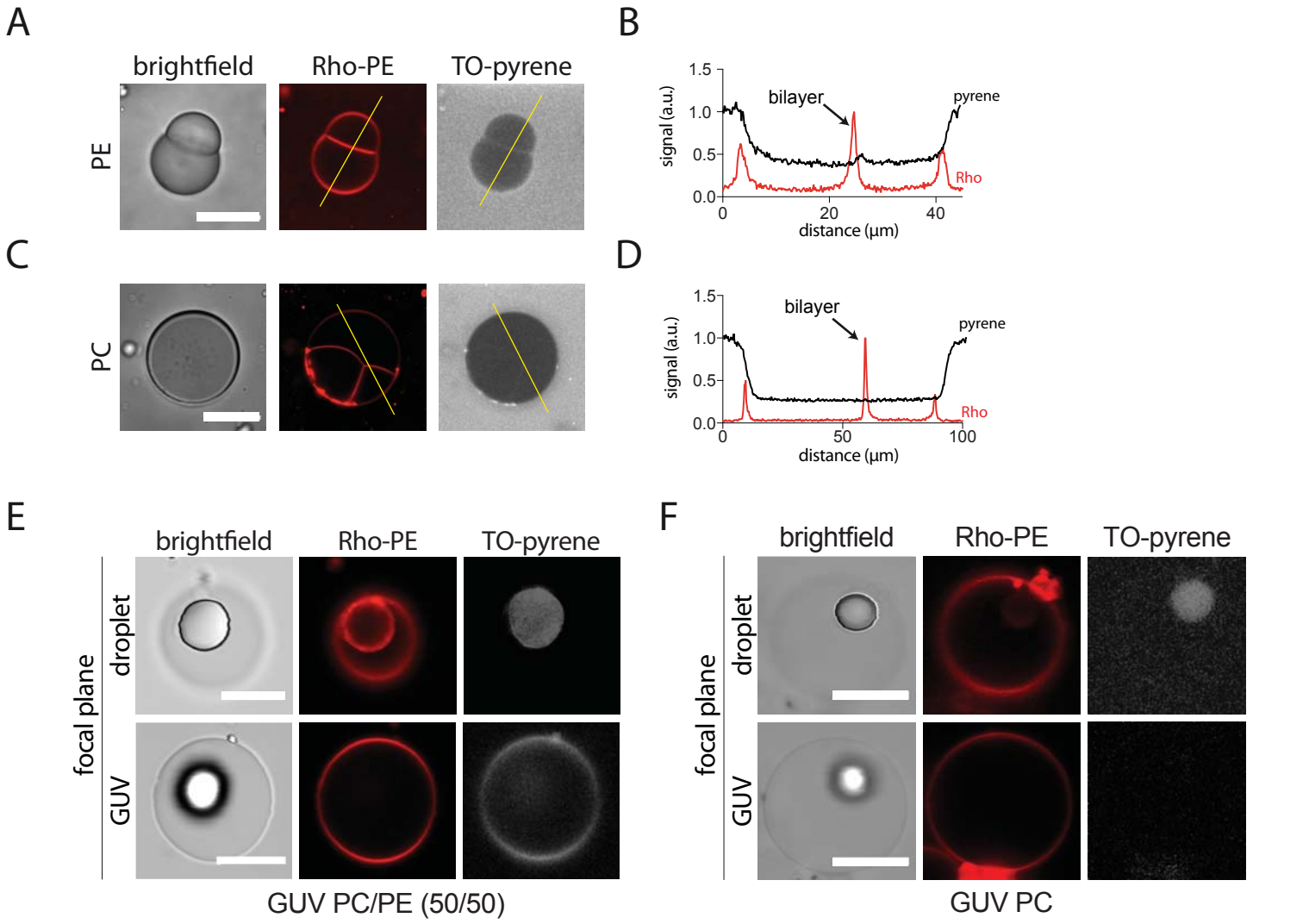

Figure S3

Ben M'Barek et al. 2016

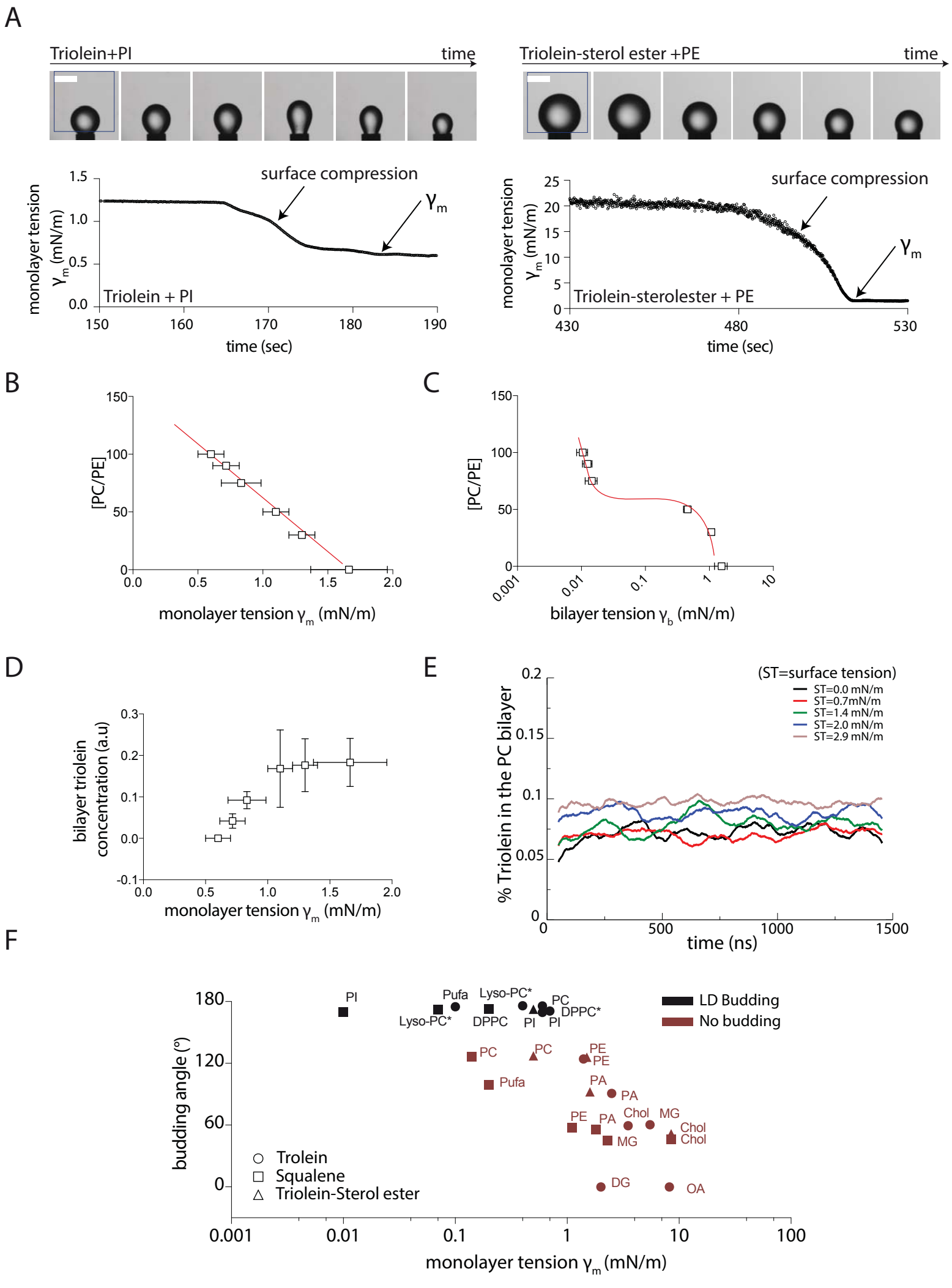

Figure S4

Ben M'Barek et al. 2016

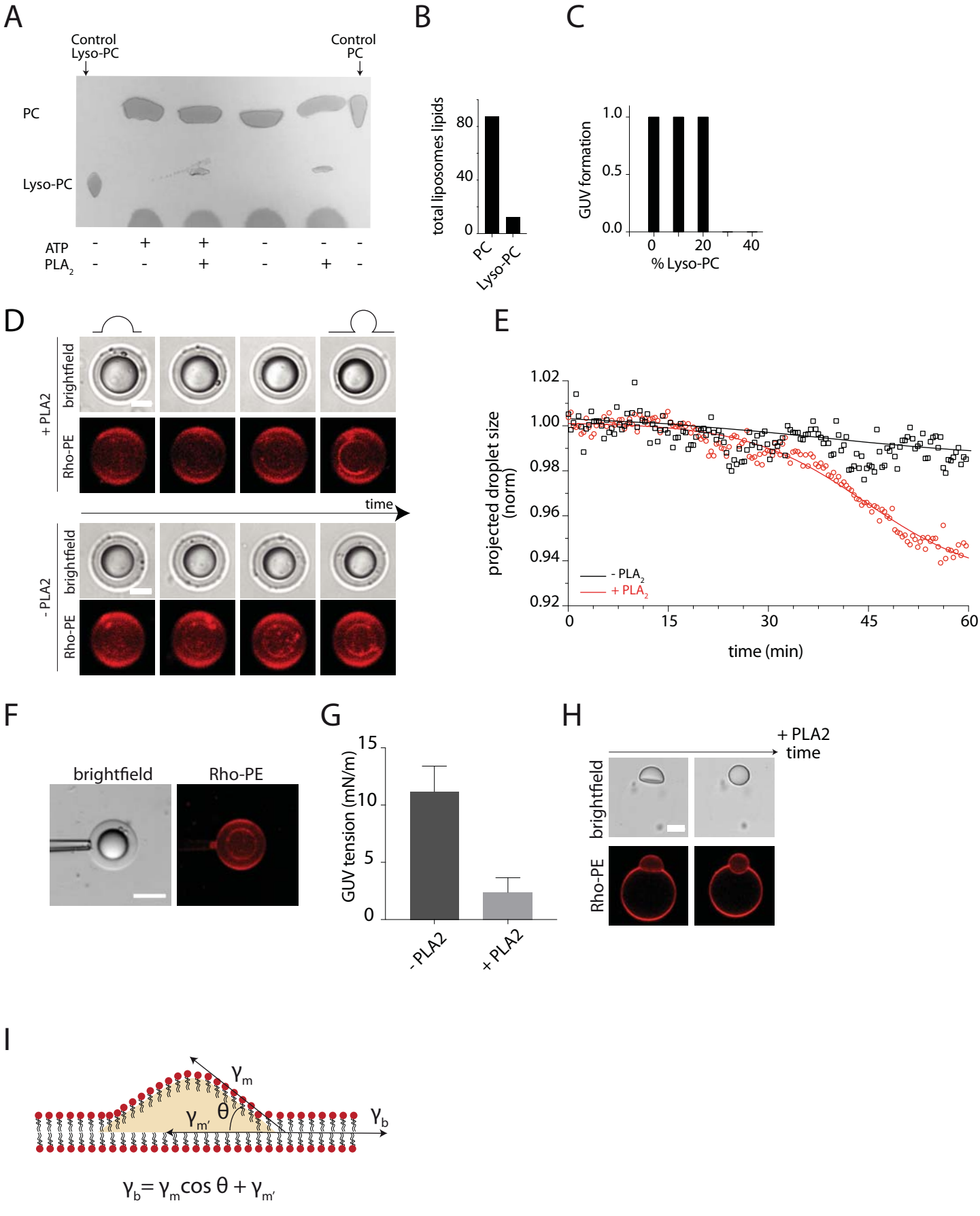

Figure S5

Ben M'Barek et al. 2016

A

Inhibited enzyme	Phenotype	Affected lipid surfactants	
LPCAT1,2		Lyso-PC	(Moessinger et al. 2014)
PLD		PA, PC	(Andersson et al. 2006; Nakamura et al. 2005)
PLC	——	PC, DG	——
$cPLA_2$	Distorted ER (TAG accumulation in the ER)	PC, Lyso-PC	(Guijas et al. 2014; Gubern et al. 2008)
SCD1		PL saturation	(Ralston & Mutch 2015; Shi et al. 2013)
Lyso PLD	——	Lyso-PA, Lyso-PC	——
AGPAT	——	PA	——
Lipin1	(TAG accumulation in the ER) ;	PLs, DG	(Guijas et al. 2014; Sembongi et al. 2013; Adeyo et al. 2011)
Seipin	;	PA, PL saturation	(Boutet et al. 2009; Fei et al. 2008; Szymanski et al. 2007)
FIT2		DG	(Gross et al. 2011; Kadereit et al. 2008)
CCT1		PC	(Krahmer et al. 2013)
ECT1	——	PC, PE	——
PEMT	Inhibition of TAG accumulation	PC, PE, PS	(Noga et al. 2002; Hörl et al. 2011)
LPAAT		PA, LPA	(Ayciriex et al. 2012)

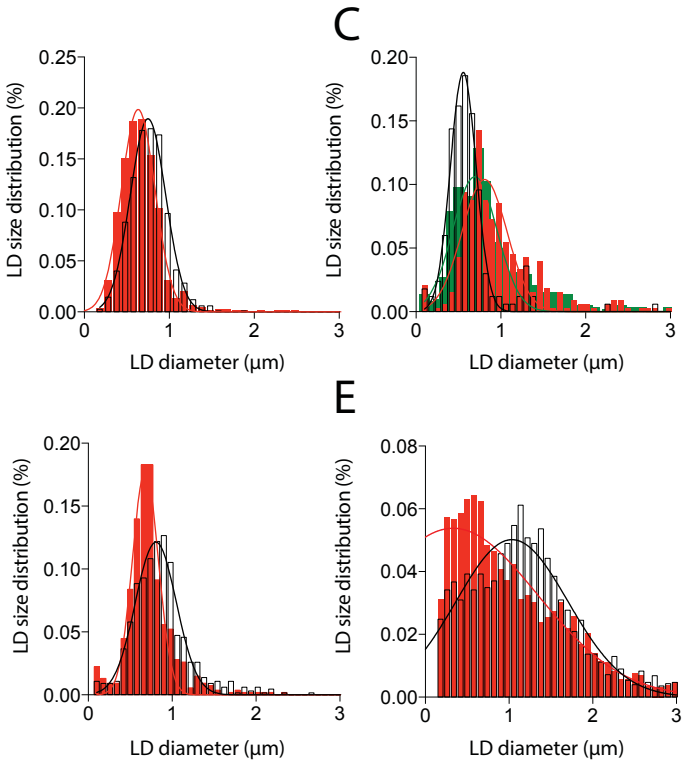

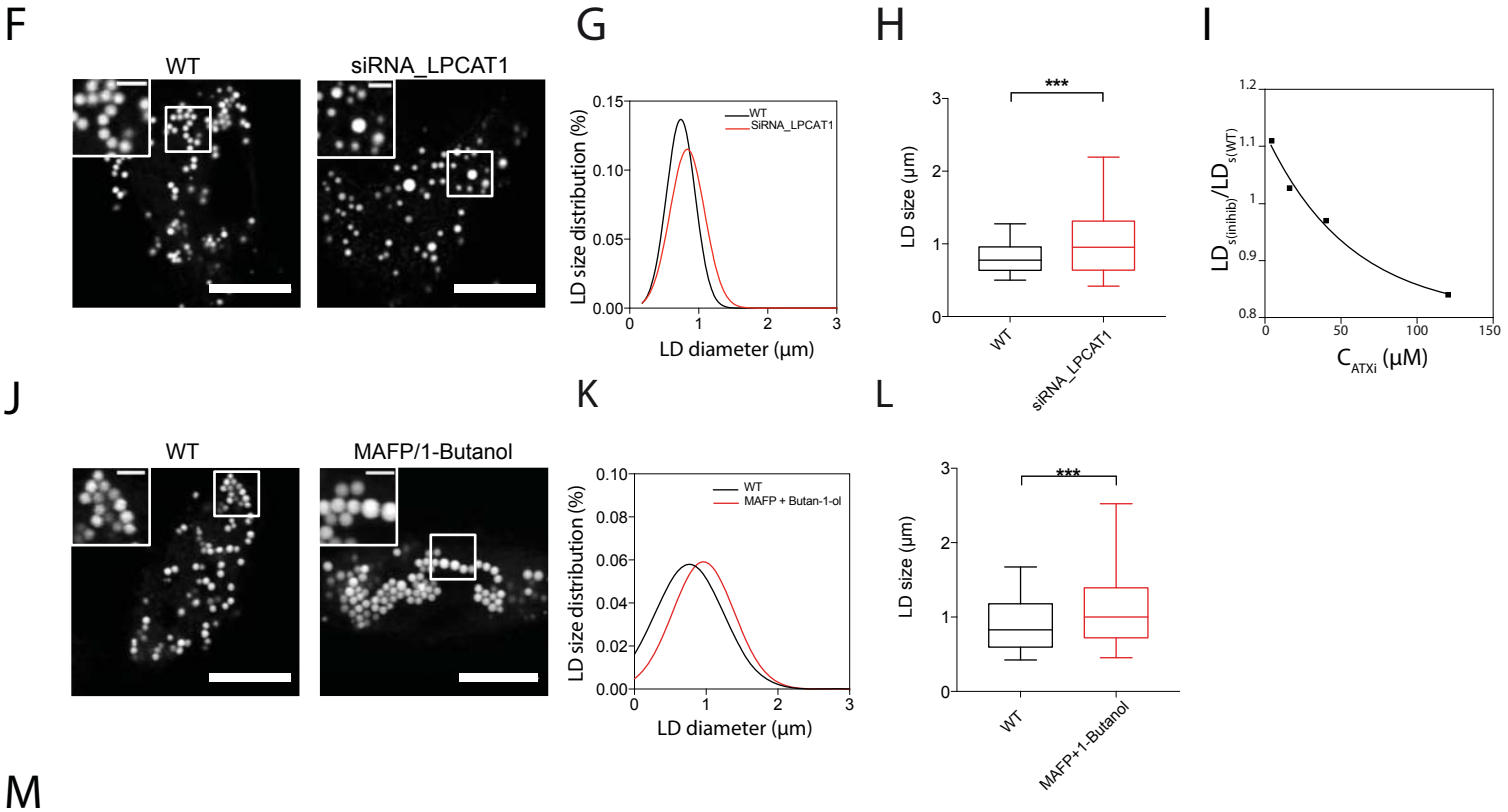

M